Optical Materials xxx (xxxx) xxx

Contents lists available at ScienceDirect

Optical Materials

journal homepage: www.elsevier.com/locate/optmat

Understanding the impact of SrI_2 additive on the properties of Sn-based halide perovskites

Hurriyet Yuce [a,b], Carlo A.R. Perini [a], Juanita Hidalgo [a], Andrés-Felipe Castro-Méndez [a], Caria Evans [a], Pablo Franco Betancur [a,c], Jacob N. Vagott [a], Yu An [a], Kathryn Bairley [a], Mustafa M. Demir [b], Juan-Pablo Correa-Baena [a,*]

[a] School of Materials Science and Engineering, Georgia Institute of Technology, North Ave NW, Atlanta, GA, 30332, USA
[b] Department of Materials Science and Engineering, Izmir Institute of Technology, 35430, Urla, Izmir, Turkey
[c] Universidad Pontificia Bolivariana, Medellin, Colombia

ARTICLE INFO

Keywords:
Halide perovskites
Lead free
Structure-property

ABSTRACT

Organic-inorganic halide perovskites have been identified as favorable candidates for the next generation of photovoltaics. Adding alkali metal halides to perovskite films has been shown to be a viable option to improve the perovskite film quality and to modulate their fundamental properties. In this work, we perform optical and electron-beam based characterizations of mixed Sn/Pb based perovskite films to investigate the effect of the addition of the alkaline metal halide SrI_2. By analyzing structural (X-ray diffraction), morphological (Scanning Electron Microscopy), optical (photoluminescence), and chemical properties (X-ray photoelectron spectroscopy), we show a complex interplay of effects upon addition of Sr^{2+} into the perovskite solution. Low concentrations of Sr^{2+} increases lattice strain, which hints at incorporation of the additive into the perovskite lattice and improves the film optoelectronic properties. As the additive concentration increases beyond 0.5 mol %, microstrain decreases. At concentrations >0.5 mol %, Sr^{2+} induces significant reduction of the average domain size, which impacts both structural and optical properties of the perovskite film.

1. Introduction

Organic-inorganic halide perovskites (ABX_3, where A = organic, B = metal, X = halide) have attracted attention as promising materials for photovoltaic applications owing to their low cost, high performance, and ease of fabrication [1,2]. The power conversion efficiency (PCE) of lead halide perovskite solar cells has rapidly improved from 3.8% in 2009 [3] to 25.5% in 2021 [4]. However, lead halide perovskites use toxic lead as the B site. More environmentally friendly alternatives are possible, which substitute Pb for Sn [5], Ge[6] or mixed metals, such as Sn/Ge [7], Pb/Sn[8,9] or Pb/Sn/Cu [10]. Alloying the B site hast the further advantage of enabling band gaps below 1.5 eV, which is desirable to maximize PCEs of solar cells [11]. As an example, mixing Sn and Pb at the B-site of perovskite allows the band gap to change from 1.17 to 1.55 eV[12].

Halide perovskites based on Sn suffer from oxidation of Sn^{2+} to Sn^{4+} when exposed to ambient conditions [13], which heavily impact their optoelectronic properties and the solar cell PCE. Considering the standard redox potentials (E_o) of Sn and Pb oxidation states, E_o (Sn^{2+}/Sn^{4+}) = 0.15 V and E_o (Pb^{2+}/Pb^{4+}) = 1.67 V, Sn oxidation is more likely to occur in comparison to the oxidation of Pb^{2+} to Pb^{4+}[14]. The oxidation results in the disruption of charge neutrality of the perovskite and destabilizes its structure [15]. The uncontrolled Sn^{2+} oxidation results in high doping densities, which induce lower charge-carrier lifetimes, increased recombination losses and shortened charge-carrier diffusion lengths, decreasing the overall performances of Sn-based optoelectronic devices [16,17]. However, the addition of SnF_2 in the perovskite precursor solution can prevent this undesired oxidation process [18,19] and this addition has shown to enhance and stabilizing the solar cell performances of Sn-containing perovsites [14,20,21]. However, according to some reports, the excessive addition of SnF_2 leads to pinhole formation in Sn-based perovskite films, and negatively affects photovoltaic performance in the devices [22,23]. Other additives such as Ag [24], ascorbic acid [25], ionic imidazolium tetra-fluoroborate ($IMBF_4$) in addition to SnF_2 antioxidant [26] have also been used to mitigate the Sn oxidation and to enhance the stability and device

* Corresponding author.
E-mail address: jpcorrea@gatech.edu (J.-P. Correa-Baena).

https://doi.org/10.1016/j.optmat.2021.111806
Received 1 July 2021; Received in revised form 1 November 2021; Accepted 15 November 2021
Available online 22 November 2021

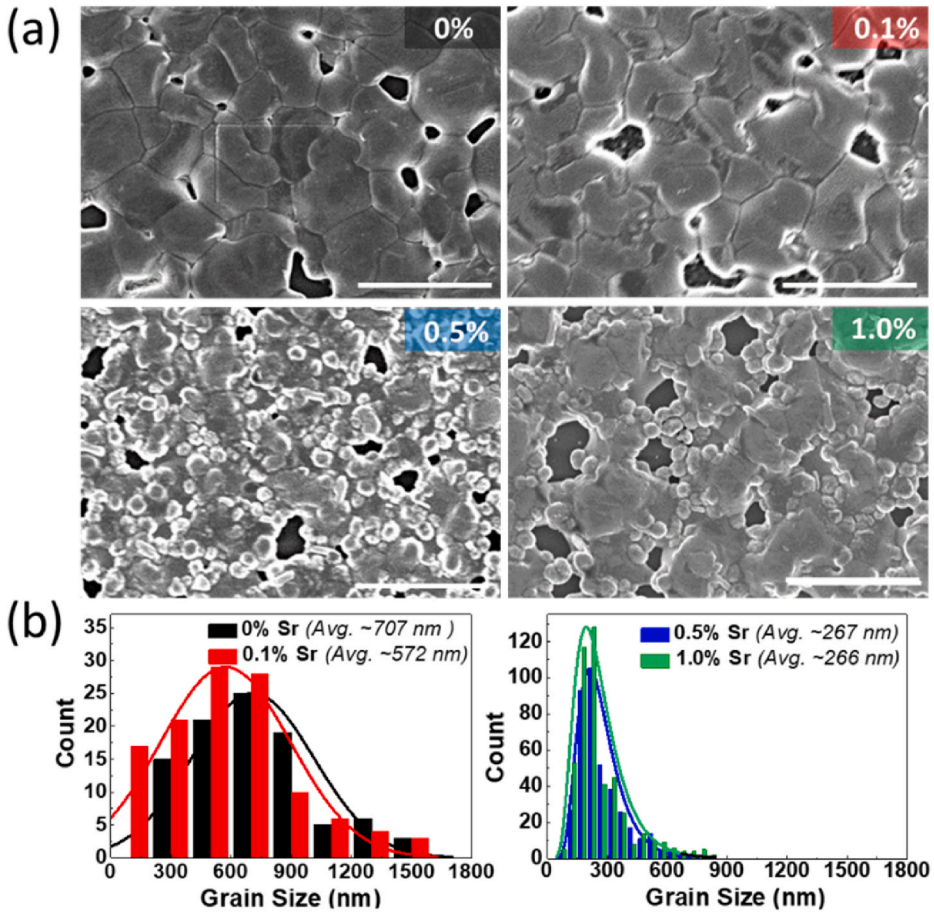

Fig. 1. (a) SEM images (Scale bar: 2 μm) and (b) Domain size distributions of $(FASnI_3)_{0.8}(MAPbBr_3)_{0.2}$ perovskite films with the addition of 0%, 0.1%, 0.5%, and 1.0% SrI_2.

performance. While these works have shown that Sn perovskites can be made more stable via additives, it is still unclear whether the observed performance improvement stems from the passivation of the Sn perovskite or from a doping effect.

In this work, we aim to understand the role of additive the SrI_2 on a Sn-based perovskite. The Sr^{2+} (118 p.m.) ion has a similar ionic radius to those of Sn^{2+} [27] and Pb^{2+} (119 p.m.) [28], which should ease its insertion into the perovskite lattice. The perovskite composition was chosen to be $(FASnI_3)_{0.8}(MAPbBr_3)_{0.2}$, to exploit the optimal band gap of ~1.4 eV for single junction solar cells. We investigated the structural and optical properties of the perovskite films with SrI_2 additive. X-ray Diffraction (XRD) was employed to investigate the structural features of perovskite films. Williamson-Hall analysis of the XRD and Urbach energy calculations from UV–vis spectra suggest two different behaviors of SrI_2 when it is added to the perovskite solution, in which the concentration of SrI_2 determines the switch between the two. At low amounts SrI_2 seems to incorporate in the perovskite structure, whereas at high amounts SrI_2 seems to segregates at the domain boundaries and surface of the perovskite film. These results are important in the quest to stabilize and passivate Sn-based perovskite films to achieve less toxic photo-absorbers with an optimal band gap for single junction perovskite solar cells.

2. Experimental section

2.1. Chemicals

Methylammonium bromide (CH_3NH_3Br) and formamidinium iodide ($CH(NH_2)_2I$) were purchased from Dyenamo. Tin iodide (SnI_2) and strontium iodide (SrI_2) were purchased from Alfa Aesar. Dimethylformamide (DMF) and dimethyl sulfoxide (DMSO) were purchased from Acros Organics. Lead bromide ($PbBr_2$) was bought from TCI America, and tin fluoride (SnF_2) was obtained from Sigma Aldrich.

2.2. Perovskite film fabrication

2.5 cm × 2.5 cm glass and FTO glass substrates were ultrasonically cleaned in 2% Hellmanex solution in water, then in DI water, acetone, and IPA, in that order. 1.5 M SnI_2 and $PbBr_2$ powders were dissolved separately in DMF/DMSO (4:1) solvent, and 10% mol SnF_2 was added to the SnI_2 solution. FAI and MABr powders were dissolved in the SnI_2 and $PbBr_2$ solutions, respectively. By mixing the Sn and Pb containing solutions, a 1.2 M $(FASnI_3)_{0.8}(MAPbBr_3)_{0.2}$ final perovskite solution was obtained. Finally, SrI_2 powder was dissolved in DMSO at a concentration of 1.0 M, and added to the final perovskite solution to achieve molar ratios (SrI_2 to Pb/Sn) of 0.1, 0.5, 1.0, 2.0 and 5.0%. The perovskite solution was deposited on glass substrates by two-step spin coating: first at 1000 rpm for 5 s and then 4000 rpm for 30 s. During spin coating, 2.5–3 mL of diethyl ether were dropped on the substrate 20 s after the program started. Then, the films were annealed at 100 °C for 15 min in a nitrogen filled glove box.

2.3. Perovskite film characterizations

Morphologies of perovskite film surfaces were obtained using the Hitachi SU-8230 scanning electron microscope (SEM). XRD measurements were carried out using a Malvern PANalytical Empyrean using Cu Kα radiation (λ= 1.54 nm) with a scan step size of 0.0131°. The chemical

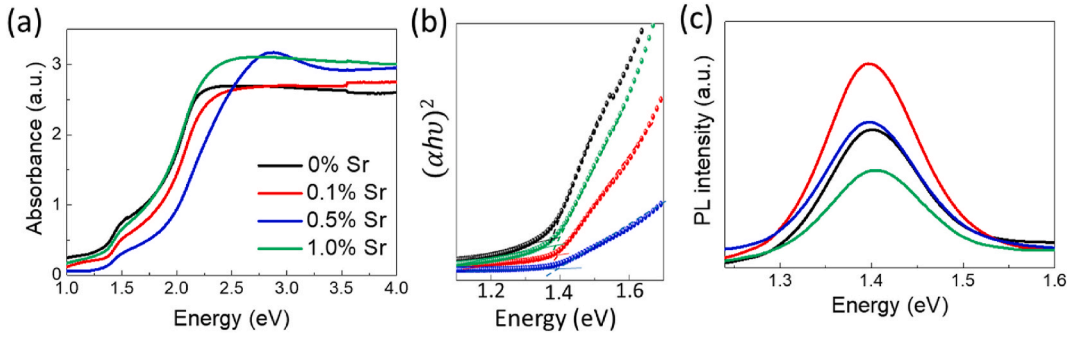

Fig. 2. Optical properties of the films. (a) UV–vis absorption, (b) Tauc Plot, and (c) PL spectra.

states of elements were probed by an XPS spectrometer (Thermo K-Alpha XPS) equipped with an Al Kα (1486.6 eV) monochromatic source with a spot size of 400 μm. Absorption spectra were collected using a Carry 500 UV–Visible–NIR spectrometer. Hyperspectral PL (Photon etc) measurements were performed by excitation using a Nd:YAG laser light the samples at 532 nm. SEM and XPS analyses were carried out on perovskite–coated FTO/glass substrates, whereas XRD and optical measurements were performed on perovskite coated glass substrates. A SnI_2 film for XRD measurements was coated in the same conditions with perovskite films on glass substrate, which served as reference.

3. Results and discussion

To observe how SrI_2 addition affects the Sn/Pb perovskite film morphology, scanning electron microscopy (SEM) was performed. The images of the perovskite films processed with different amounts of SrI_2, ranging from 0% to 1.0%, are shown in Fig. 1a. The images show markedly different morphologies, with smaller domains forming as SrI_2 concentration increases. Even though smaller domains are formed and the number of small domains increases, there are still large domains present in the film for concentrations up to 2.0% SrI_2. When increasing the concentration from 2.0% to 5.0%, all large domains completely disappear and the number of pinholes significantly decreases (Fig. S1) . In addition to the reduction of average domain size, the area of pinholes also shrinks with the increasing SrI_2 amount in the films. The pinholes originate from fast crystallization in the film during the annealing process, which changes with the addition of SrI_2[27]. The distributions of domain size for the perovskite films are shown in Fig. 1b. Domain sizes of the perovskite film without SrI_2 vary from nearly 1.6 μm to 0.2 μm. When adding 0.1% SrI_2 to the perovskite, the average domain size of the perovskite films decreased from ~707 nm to ~572 nm, and the distribution narrowed significantly. When the SrI_2 additive concentration in the film was 0.5% and above, we observed that the domain sizes further decreased, with the 5.0% SrI_2 showing ~157 nm average domain diameter (Fig. S1).

Optical absorbance analysis of pristine and SrI_2 added to the $(FASnI_3)_{0.8}(MAPbBr_3)_{0.2}$ perovskite films were carried out for the energies between 1.0 and 4.0 eV as shown in Fig. 2a. From the absorbance spectra of the perovskite films, the optical band gap (E_g) was calculated using the Tauc's plots [29] shown in Fig. 2b using the formula $h\upsilon = \beta(h\upsilon - E_g)^x$; where x = ½ for a direct band gap material. In the equation, α, $h\nu$, and β are absorption coefficient, the energy of the photon, and a constant, respectively. The optical band gap energies retrieved for all films are ~1.4 eV. To further understand the effect of SrI_2 on the optical properties of Sn containing perovskite films, we performed PL measurements (Fig. 2c). The PL peaks of all perovskite films are located at ~1.4 eV. The highest emission intensity among the perovskite films belongs to the perovskite film with 0.1% SrI_2, while the PL intensities of the 0.5% SrI_2 perovskite film decreases, albeit higher than that of the pristine perovskite film. The results show that SrI_2 at different concentrations in the perovskite films improves the emission intensities of these perovskite materials. Compared to the other perovskite films, 1.0% Sr added perovskite film has the lowest PL intensity. When we compare the absorptions of the films between 1.5 eV and 2.25 eV in the visible region, the 0.5% Sr perovskite film shows lower absorption which suggests lower thickness compared to the other perovskite films. Therefore, PL intensities of 0.1% and 0.5% Sr added perovskites cannot be directly compared due to the difference in the thickness. However, we can say that Sr addition at $\leq$ 0.5% concentration to the perovskite improves the optical properties of the perovskite film.

To understand the impact of the SrI_2 additive on the crystal structure of the $(FASnI_3)_{0.8}(MAPbBr_3)_{0.2}$ perovskite, XRD was measured and the results are shown in Fig. 3a. The signals at 2θ of 14.1, 24.6, 28.4, 31.9, 40.7, and 43.3° correspond to the characteristic diffraction peaks of the $(FASnI_3)_{0.8}(MAPbBr_3)_{0.2}$ perovskite [30,31]. In addition, the pristine and 0.1% SrI_2 perovskite films include excess SnI_2 signals at 2θ of 12.6, 25.5, 38.7, and 52.5°. No additional crystalline phases were formed upon addition of different SrI_2 amounts into the perovskite. The addition of 0.1% SrI_2 is shown to decrease the excess SnI_2 signal. At 0.5% SrI_2, the excess SnI_2 signature completely disappears and the perovskite film

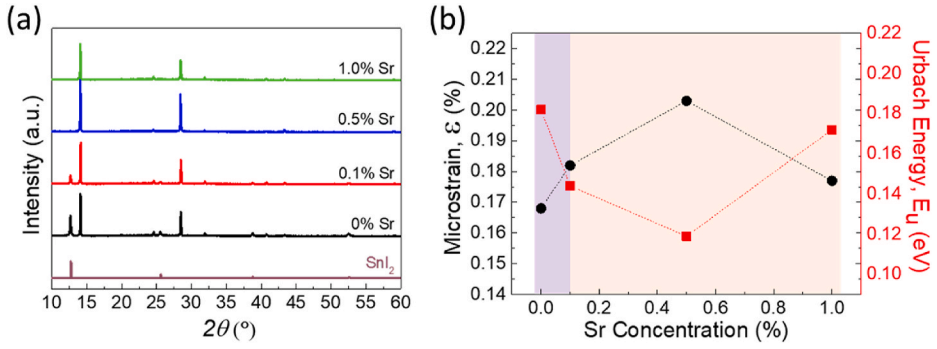

Fig. 3. (a) XRD pattern and (b) microstrain and Urbach energies of the perovskite films with varying SrI_2 concentrations.

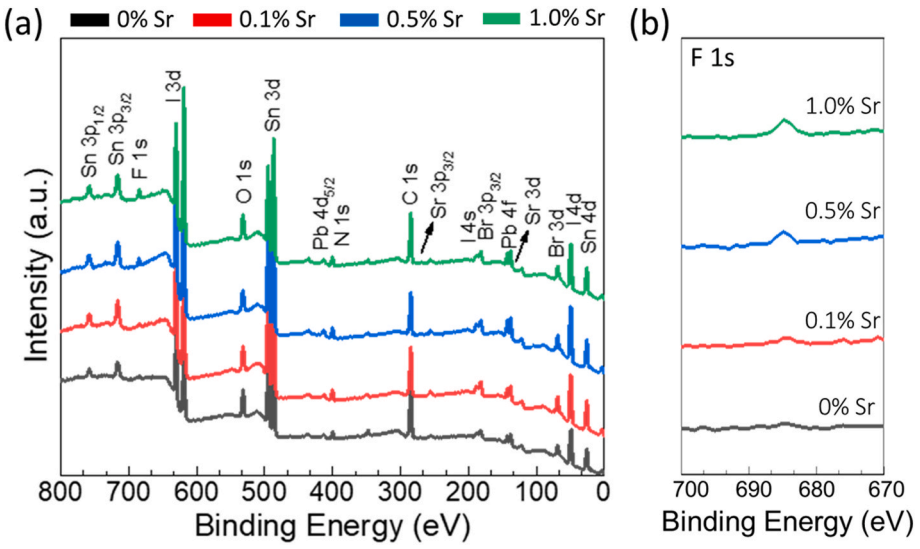

Fig. 4. (a) X-ray photoelectron spectroscopy overview spectra and (b) F 1s peaks of the perovskite films.

exhibits the highest XRD peak intensity for the perovskite phase. When the concentration of SrI_2 is increased from 0.5% to 1.0%, the intensities of the XRD peaks for the perovskite structure decrease. The XRD results show that SrI_2 additive significantly increases the perovskite peak intensity until 0.5%. The crystallite size calculated by Williamson–Hall method of the perovskites is also increased by the addition of SrI_2 until 0.5% (Figs. S3–S4).

We calculated microstrain (Figs. 3b and S3) within the perovskite lattice using the Williamson-Hall plot method, which utilizes full width at half-maximum (FWHM) of XRD signals. When SrI_2 is introduced in the perovskite precursor solution at low concentrations (below 0.5%) an increase in microstrain is observed up to 0.5%, because of the distortion of the lattice due to Sr^{2+} incorporation. Above 0.5% SrI_2, the decrease in microstrain results from the segregation of SrI_2 and lack of Sr^{2+} incorporation, as high concentrations of SrI_2 can lead to precipitate formation. Similar behavior of SrI_2 related to doping and segregation of Sr^{2+} was observed by Phung et al. with introduced Sr^{2+} at low concentrations to a $MAPbI_3$ perovskite solution [32]. They observed Sr^{2+} segregation beyond 0.2% SrI_2 added $MAPbI_3$ while we observed the segregation beyond 0.5% SrI_2 added $(FASnI_3)_{0.8}(MAPbBr_3)_{0.2}$ perovskite films. The reason for this difference is possibly originated from rapid crystallization of Sn-based perovskites[33] and entrapment of Sr^{2+} ions within the

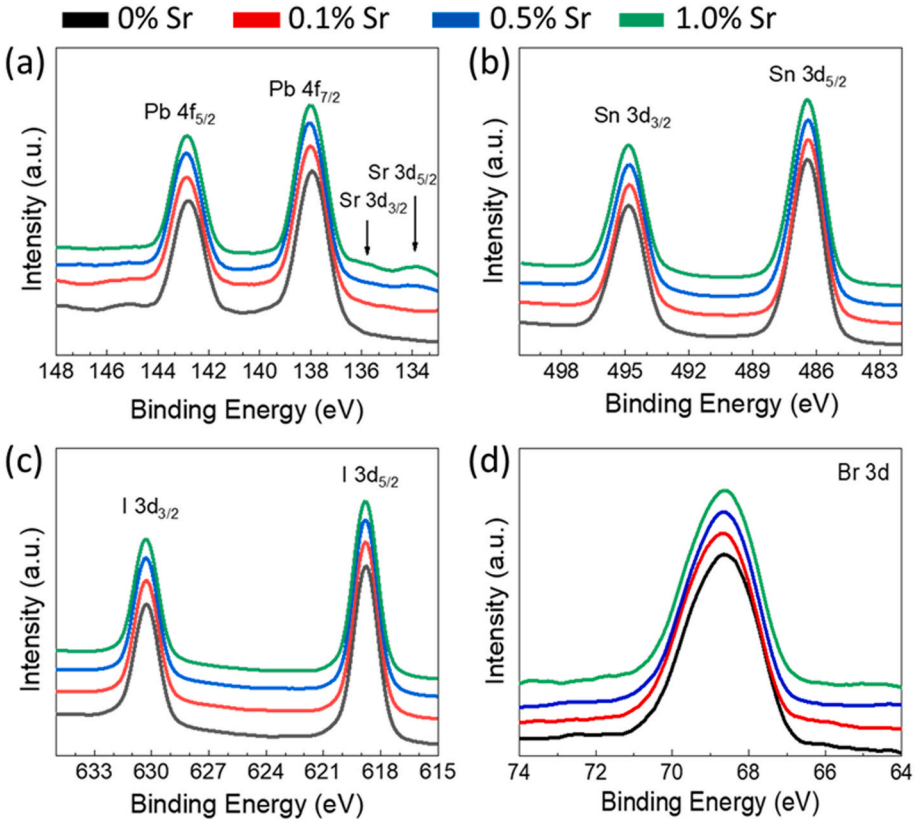

Fig. 5. XPS spectra of (a) Pb 4f and Sr 3d, (b) Sn 3d, (c) I 3d, and (d) Br 3d in the perovskite films.

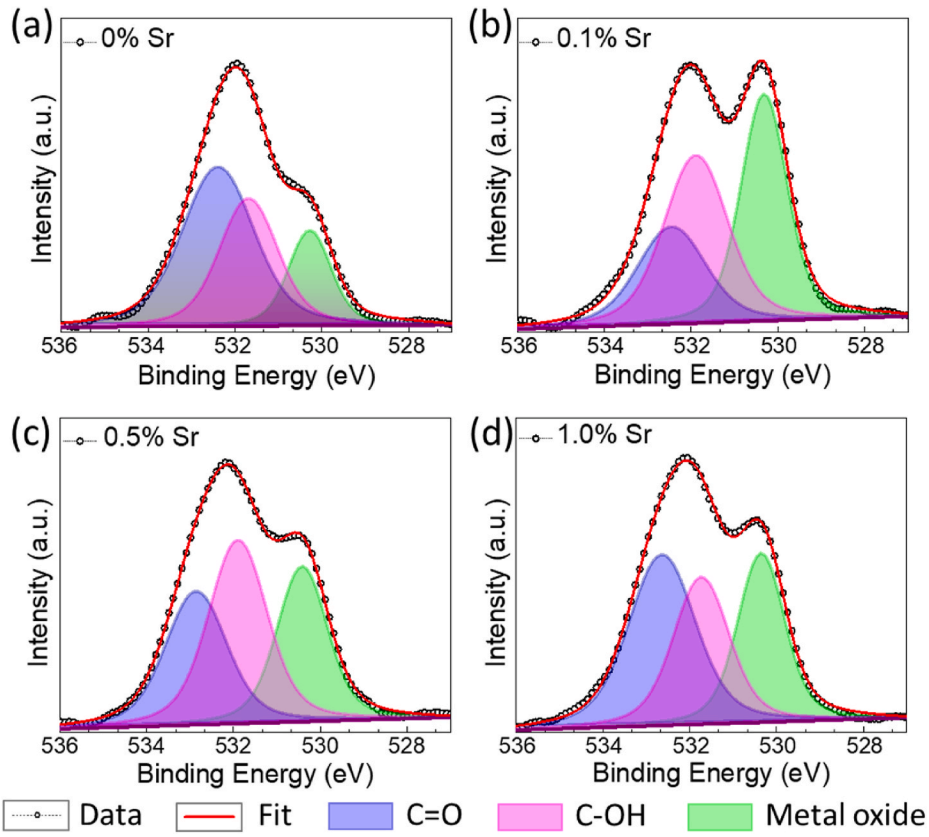

Fig. 6. XPS spectra of O 1s peaks of (a) pristine (b) 0.1% (c) 0.5%, and (d) 1.0% SrI_2 added perovskite films.

lattice. However, a high concentration of SrI_2 (e.g. 5%) additive may result in stress in the perovskite lattice (Fig. S5). This can be a result of the segregation of dopants at the domain boundaries since the higher doping concentrations cause a disturbance in the long-range crystallographic ordering [34]. However, we did not observe a difference between doped and segregated Sr^{2+} effects on the morphology of the perovskite films apart from the effect of SrI_2 additives on the domain size (Fig. 1). SrI_2 addition to the perovskite could also lead to a higher concentration of nucleation sites, which results in smaller domains for both doping and segregation mechanism as shown in Fig. 1, which are in agreement with what observed by Pérez-del-Rey et al. [35] and by Wang et al. [36], respectively.

We calculated the Urbach energies for the samples for comparison to the structural disorder in the perovskite films as shown in Fig. 3b (details in Fig. S6). The Urbach energy decreases with the addition of SrI_2 and reaches the lowest value when $\leq$ 0.5%, which is ascribed to higher electronic quality the addition of SrI_2. Above 0.5% SrI_2, the Urbach energy increases likely due to the segregation of SrI_2, as suggested by the microstrain analysis, however, it is still lower than that of the pristine perovskite. For 5.0%, a larger drop in Urbach energy is shown, suggesting that segregated SrI_2 have a beneficial effect on the structural and electronic properties of the perovskite polycrystalline films (Fig. S5). Other researchers have suggested that accumulation of metal halides at the surface of the crystalline domain act as a passivation layers [37–39]. It is possible that this is happening in these polycrystalline thin films only when the SrI_2 concentration is high enough to induce segregation, then passivating the surface of the perovskite. Both microstrain and Urbach energy show that large changes in the structure and electronic defects are happening at 5.0% SrI_2 (Fig. S5). The former can be attributed to the changes in the morphology with small domains [36] and the latter with those smaller domains being passivated by the SrI_2 at higher proportion than in lower SrI_2 concentrations. Urbach energies are different for each sample while band gaps of the films remain unchanged.

In order to investigate the effect of SrI_2 additive on the elemental composition of the $(FASnI_3)_{0.8}(MAPbBr_3)_{0.2}$ perovskite, XPS analyses were carried out in the range of 0–800 eV as shown in Fig. 4. According to the XPS survey results, the elements identified on the surface of perovskite films are Sn, F, O, C, N, Pb, Br, I, and Sr. C, N, Pb, Sn, Br, and I come from the chemical composition of perovskite films. F and Sr peaks are originated from added SnF_2 and SrI_2 to the perovskite solution, respectively. The O peak can be attributed to a combination of metal oxides and adsorbed oxygen. After adding SrI_2 to the perovskite structure, the F 1s peak at ~684.7 eV appears and the intensity of the peak increases for higher SrI_2 concentrations (Fig. 4b). Interestingly, these results suggest that the SrI_2 additive leads to the accumulation of F on the surface of the perovskite films. This accumulation trend is most probably originated from the phase segregation of SnF_2, and the brightness on the SEM images in Fig. 1 can be attributed to the segregation of F [40,41].

We performed high resolution XPS of the Sn 3d, Pb 4f, I 3d, and Br 3d spectra as shown in Fig. 5. The Sn 3d spectra for pristine and SrI_2 added $(FASnI_3)_{0.8}(MAPbBr_3)_{0.2}$ perovskite films show $3d_{3/2}$ and $3d_{5/2}$ peaks at 494.8 and 486.3 eV (Fig. 5b) [42], respectively. The Pb 4f spectra exhibit $4f_{5/2}$ and $4f_{7/2}$ peaks at 142.7 and 137.9 eV (Fig. 5a) [32], respectively. The I 3d spectrum for the films have $3d_{3/2}$ and $3d_{5/2}$ peaks at 630.2 and 618.7 eV (Fig. 5c) [43], respectively. The Br 3d peak is observed at 68.6 eV (Fig. 5d) [44]. The presence of Sr in the perovskite films are not very clear in the Pb 4f –Sr3d XPS data in the range of 148 eV and 133.5 eV due to low concentration of Sr additive (Fig. 5a). Above 1% of Sr concentration, Sr 3d signal in XPS is clearly seen in Fig. S8. The Sr $3d_{3/2}$ (135.6 eV) and Sr $3d_{5/2}$ (133.9 eV) are located in Pb 4f spectra in Fig. S8[43]. After the addition of SrI_2 to the perovskite, Pb 4f, I 3d, Sr 3d, and Br peaks shift to higher binding energies. The reason for these shifts could be the presence of an oxide owing to surface band-bending [45]. These shifts in XPS peaks suggest the chemical structure modification of

the surface in the perovskite films [43].

In order to understand the effect of SrI_2 on oxygen interactions at the surface, the O 1s core-level spectra were deconvoluted into three oxygen-binding states corresponding to metal oxides (Sn–O, Pb–O, or Sr–O), C–OH, and C═O in Fig. 6. The binding energies of the oxygen fitted peaks are observed at 530.26, 531.68 and 532.38 eV which are assigned to metal oxide coming from either Sn–O, Pb–O and/or Sr–O, and C–OH and C═O, respectively. The latter two due to adsorbed atmospheric hydrocarbons from air [46–48]. When we examine deconvolution of O 1s spectra, the atomic ratio of the metal oxide species for pristine perovskite film is 17.71%. When adding 5.0% SrI_2 to the perovskite solution, the atomic percent of the metal oxide species decreases to 8.83% as shown in Figs. S9 and S10. Fig. 6 reveals that metal oxidation at the surface increases as more Sr is present, suggesting that SrOx is forming, which could act as passivation layer.

4. Conclusions

We have presented a detailed investigation of the effects of SrI_2 addition to $(FASnI_3)_{0.8}(MAPbBr_3)_{0.2}$ perovskite thin films. We showed that the SrI_2 additive leads to Sr incorporation in the perovskite for 0.1 and 0.5% SrI_2 concentrations. For higher concentrations, SrI_2 segregation takes place in the perovskite owing to the lattice relaxation with lower strain. Urbach energy calculations of the perovskite films show that SrI_2 addition leads to increased electronic quality in both Sr^{2+}-incorporated and SrI_2 segregation cases. These results suggest segregated SrI_2 in the film could be acting as a passivating agent when at high enough concentrations exceeding the doping limit of 0.5%. The SrI_2 addition was shown to increase metal oxide content in the surface and could therefore act as a passivant while also increasing long-term durability of these lead-free materials.

CRediT authorship contribution statement

Hurriyet Yuce: Conceptualization, Methodology, Software, Data curation, Writing – original draft. **Carlo A.R. Perini:** Methodology, Software, Data curation. **Juanita Hidalgo:** Methodology, Software, Data curation. **Andrés-Felipe Castro-Méndez:** Methodology, Software, Data curation. **Caria Evans:** Methodology, Software, Data curation. **Pablo Franco Betancur:** Methodology, Software, Data curation. **Jacob N. Vagott:** Methodology, Software, Data curation. **Yu An:** Methodology, Software, Data curation. **Kathryn Bairley:** Methodology, Software, Data curation, Methodology, Software, Data curation. **Mustafa M. Demir:** Supervision. **Juan-Pablo Correa-Baena:** Supervision, Conceptualization, Methodology, Data curation.

Declaration of competing interest

The authors declare that they have no known competing financial interests or personal relationships that could have appeared to influence the work reported in this paper.

Acknowledgments

This work was performed in part at the Georgia Tech Institute for Electronics and Nanotechnology, a member of the National Nanotechnology Coordinated Infrastructure (NNCI), which is supported by the National Science Foundation (Grant ECCS-1542174) and Council of Higher Education of Turkey (CoHE)-YUDAB Research Scholarship. H.Y. thanks Yenal Yalcinkaya for insightful discussions. JPCB is partly funded by the Goizueta Foundation.

J.P.C.B., Y.A., C.A.R.P., J.H., A.F.C.M., J.N.V., and C.E. thank Georgia Institute of Technology for the financial support.

Appendix A. Supplementary data

Supplementary data to this article can be found online at https://doi.org/10.1016/j.optmat.2021.111806.

References

[1] J.-P. Correa-Baena, M. Saliba, T. Buonassisi, M. Grätzel, A. Abate, W. Tress, A. Hagfeldt, Promises and challenges of perovskite solar cells, Science (80-.) 358 (2017) 739–744.
[2] B. Zhang, J. Yan, J. Wang, Y. Chen, Effect of the modulating of organic content on optical properties of single-crystal perovskite, Opt. Mater. (Amst). 62 (2016) 273–278.
[3] A. Kojima, K. Teshima, Y. Shirai, T. Miyasaka, Organometal halide perovskites as visible-light sensitizers for photovoltaic cells, J. Am. Chem. Soc. 131 (2009) 6050–6051.
[4] Best Research-Cell Efficiency Chart | Photovoltaic Research | NREL (accessed Jan 10, 2021), https://www.nrel.gov/pv/cell-efficiency.html.
[5] T.M. Koh, T. Krishnamoorthy, N. Yantara, C. Shi, W.L. Leong, P.P. Boix, A. C. Grimsdale, S.G. Mhaisalkar, N. Mathews, Formamidinium tin-based perovskite with low Eg for photovoltaic applications, J. Mater. Chem. A 3 (2015) 14996–15000.
[6] N. Lakhdar, A. Hima, Electron transport material effect on performance of perovskite solar cells based on CH3NH3GeI3, Opt. Mater. (Amst). 99 (2020) 109517.
[7] M. Chen, M.G. Ju, H.F. Garces, A.D. Carl, L.K. Ono, Z. Hawash, Y. Zhang, T. Shen, Y. Qi, R.L. Grimm, D. Pacifici, X.C. Zeng, Y. Zhou, N.P. Padture, Highly stable and efficient all-inorganic lead-free perovskite solar cells with native-oxide passivation, Nat. Commun. 10 (2019) 16.
[8] Y. Zong, Z. Zhou, M. Chen, N.P. Padture, Y. Zhou, Lewis-adduct mediated grain-boundary functionalization for efficient ideal-bandgap perovskite solar cells with superior stability, Adv. Energy Mater. 8 (2018) 1800997.
[9] A. Wang, X. Gan, J. Yu, Simulation of narrow-bandgap mixed Pb–Sn perovskite solar cells with inverted p-i-n structure, Opt. Mater. (Amst). 112 (2021) 110751.
[10] M. Li, Z.K. Wang, M.P. Zhuo, Y. Hu, K.H. Hu, Q.Q. Ye, S.M. Jain, Y.G. Yang, X. Y. Gao, L.S. Liao, Pb–Sn–Cu ternary organometallic halide perovskite solar cells, Adv. Mater. 30 (2018) 1800258.
[11] W. Shockley, H.J. Queisser, Detailed balance limit of efficiency of P-n junction solar cells, J. Appl. Phys. 32 (1961) 510–519.
[12] Y. Ogomi, A. Morita, S. Tsukamoto, T. Saitho, N. Fujikawa, Q. Shen, T. Toyoda, K. Yoshino, S.S. Pandey, T. Ma, S. Hayase, CH3NH3SnxPb(1-x)I3 perovskite solar cells covering up to 1060 nm, J. Phys. Chem. Lett. 5 (2014) 1004–1011.
[13] N.K. Noel, S.D. Stranks, A. Abate, C. Wehrenfennig, S. Guarnera, A.A. Haghighirad, A. Sadhanala, G.E. Eperon, S.K. Pathak, M.B. Johnston, A. Petrozza, L.M. Herz, H. J. Snaith, Lead-free organic-inorganic tin halide perovskites for photovoltaic applications, Energy Environ. Sci. 7 (2014) 3061–3068.
[14] S. Gupta, D. Cahen, G. Hodes, How SnF2 impacts the material properties of lead-free tin perovskites, J. Phys. Chem. C 122 (2018) 13926–13936.
[15] T. Leijtens, R. Prasanna, A. Gold-Parker, M.F. Toney, M.D. McGehee, Mechanism of tin oxidation and stabilization by lead substitution in tin halide perovskites, ACS Energy Lett 2 (2017) 2159–2165.
[16] R.L. Milot, M.T. Klug, C.L. Davies, Z. Wang, H. Kraus, H.J. Snaith, M.B. Johnston, L. M. Herz, The effects of doping density and temperature on the optoelectronic properties of formamidinium tin triiodide thin films, Adv. Mater. 30 (2018).
[17] D. Ricciarelli, D. Meggiolaro, F. Ambrosio, F. De Angelis, Instability of tin iodide perovskites: bulk p-doping versus surface tin oxidation, ACS Energy Lett 5 (2020) 2787–2795.
[18] C. Ran, J. Xi, W. Gao, F. Yuan, T. Lei, B. Jiao, X. Hou, Z. Wu, Bilateral interface Engineering toward efficient 2D-3D bulk heterojunction tin halide lead-free perovskite solar cells, ACS Energy Lett 3 (2018) 713–721.
[19] T. Leijtens, G.E. Eperon, N.K. Noel, S.N. Habisreutinger, A. Petrozza, H.J. Snaith, Stability of metal halide perovskite solar cells, Adv. Energy Mater. 5 (2015) 1500963.
[20] F. Gu, S. Ye, Z. Zhao, H. Rao, Z. Liu, Z. Bian, C. Huang, Improving performance of lead-free formamidinium tin triiodide perovskite solar cells by tin source purification, Sol. RRL 2 (2018) 1800136.
[21] T.S. Ripolles, D. Yamasuso, Y. Zhang, M.A. Kamarudin, C. Ding, D. Hirotani, Q. Shen, S. Hayase, New tin(II) fluoride derivative as a precursor for enhancing the efficiency of inverted planar tin/lead perovskite solar cells 122 (2018) 27284–27291.
[22] W. Liao, D. Zhao, Y. Yu, C.R. Grice, C. Wang, A.J. Cimaroli, P. Schulz, W. Meng, K. Zhu, R.G. Xiong, Y. Yan, Lead-free inverted planar formamidinium tin triiodide perovskite solar cells achieving power conversion Efficiencies up to 6.22, Adv. Mater. 28 (2016) 9333–9340.
[23] S.J. Lee, S.S. Shin, Y.C. Kim, D. Kim, T.K. Ahn, J.H. Noh, J. Seo, S. Seok, Il. Fabrication of efficient formamidinium tin iodide perovskite solar cells through SnF2–pyrazine complex, J. Am. Chem. Soc. 138 (2016) 3974–3977.
[24] C. Park, J. Choi, J. Min, K. Cho, Suppression of oxidative degradation of tin – lead hybrid organometal halide perovskite solar cells by Ag doping 5 (2020) 3285–3294.
[25] X. Xu, C.C. Chueh, Z. Yang, A. Rajagopal, J. Xu, S.B. Jo, A.K.Y. Jen, Ascorbic acid as an effective antioxidant additive to enhance the efficiency and stability of Pb/Sn-based binary perovskite solar cells, Nano Energy 34 (2017) 392–398.

[26] H. Kim, J.W. Lee, G.R. Han, S.K. Kim, J.H. Oh, Synergistic effects of cation and anion in an ionic imidazolium tetrafluoroborate additive for improving the efficiency and stability of half-mixed Pb-Sn perovskite solar cells, Adv. Funct. Mater. (2020) 1–12, 2008801.
[27] W. Qiu, T. Merckx, M. Jaysankar, C. Masse De La Huerta, L. Rakocevic, W. Zhang, U.W. Paetzold, R. Gehlhaar, L. Froyen, J. Poortmans, D. Cheyns, H.J. Snaith, P. Heremans, Pinhole-free perovskite films for efficient solar modules, Energy Environ. Sci. 9 (2016) 484–489.
[28] S.H. Chan, M.C. Wu, K.M. Lee, W.C. Chen, T.H. Lin, W.F. Su, Enhancing perovskite solar cell performance and stability by doping barium in methylammonium lead halide, J. Mater. Chem. A 5 (2017) 18044–18052.
[29] S.R. Kodigala, Cu (In1-XGax) Se2 Based Thin Film Solar Cells, Academic Press, 2011.
[30] Y. Hu, M.F. Aygüler, M.L. Petrus, T. Bein, P. Docampo, Impact of rubidium and cesium cations on the moisture stability of multiple-cation mixed-halide perovskites, ACS Energy Lett 2 (2017) 2212–2218.
[31] E.P. Yao, P. Sun, W. Huang, E.P. Yao, Y. Yang, M. Wang, Efficient planar perovskite solar cells using halide Sr-substituted Pb perovskite, Nano Energy 36 (2017) 213–222.
[32] N. Phung, R. Félix, D. Meggiolaro, A. Al-Ashouri, G. Sousa e Silva, C. Hartmann, J. Hidalgo, H. Köbler, E. Mosconi, B. Lai, The doping mechanism of halide perovskite unveiled by alkaline Earth metals, J. Am. Chem. Soc. 142 (2020) 2364–2374.
[33] S.A.U. Hasan, D.S. Lee, S.H. Im, K.H. Hong, Present status and Research prospects of tin-based perovskite solar cells, Sol. RRL 4 (2020) 1–30.
[34] V.S. Anitha, S. Sujatha Lekshmy, K. Joy, Effect of Mn doping on the structural, magnetic, optical and Electrical properties of ZrO2-SnO2 thin films prepared by sol-gel method, J. Alloys Compd. 675 (2016) 331–340.
[35] D. Pérez-del-Rey, D. Forgács, E.M. Hutter, T.J. Savenije, D. Nordlund, P. Schulz, J. J. Berry, M. Sessolo, H.J. Bolink, Strontium insertion in methylammonium lead iodide: long charge carrier lifetime and high fill-factor solar cells, Adv. Mater. 28 (2016) 9839–9845.
[36] J.T.-W. Wang, Z. Wang, S. Pathak, W. Zhang, D.W. deQuilettes, F. Wisnivesky-Rocca-Rivarola, J. Huang, P.K. Nayak, J.B. Patel, H.A.M. Yusof, Efficient perovskite solar cells by metal ion doping, Energy Environ. Sci. 9 (2016) 2892–2901.
[37] K.-C.C. Hsiao, M.-H.H. Jao, B.-T.T. Li, T.-H.H. Lin, S.H.-C.C. Liao, M.-C.C. Wu, W.-F.F. Su, Enhancing efficiency and stability of hot casting p–i–n perovskite solar cell via dipolar ion passivation, ACS Appl. Energy Mater. 2 (2019) 4821–4832.
[38] A. Rajagopal, P.-W.W. Liang, C.-C.C. Chueh, Z. Yang, A.K.Y.K.-Y. Jen, Defect passivation via a graded fullerene heterojunction in low-bandgap Pb–Sn binary perovskite photovoltaics, ACS Energy Lett 2 (2017) 2531–2539.
[39] D. Xin, S. Tie, R. Yuan, X. Zheng, J. Zhu, W.-H.H. Zhang, Defect passivation in hybrid perovskite solar cells by tailoring the electron density distribution in passivation molecules, ACS Appl. Mater. Interfaces 11 (2019) 44233–44240.
[40] X. Liu, Y. Wang, T. Wu, X. He, X. Meng, J. Barbaud, H. Chen, H. Segawa, X. Yang, L. Han, Efficient and stable tin perovskite solar cells enabled by amorphous-polycrystalline structure, Nat. Commun. 11 (2020) 2678.
[41] Z. Zhao, F. Gu, Y. Li, W. Sun, S. Ye, H. Rao, Z. Liu, Z. Bian, C. Huang, Mixed-organic-cation tin iodide for lead-free perovskite solar cells with an efficiency of 8.12, Adv. Sci. 4 (2017) 1700204.
[42] L. Huang, X. Zhou, R. Xue, P. Xu, S. Wang, C. Xu, W. Zeng, Y. Xiong, H. Sang, D. Liang, Low-temperature growing anatase TiO2/SnO2 multi-dimensional heterojunctions at MXene conductive network for high-Efficient perovskite solar cells, Nano-Micro Lett. 12 (2020) 44.
[43] C.F.J. Lau, M. Zhang, X. Deng, J. Zheng, J. Bing, Q. Ma, J. Kim, L. Hu, M.A. Green, S. Huang, A. Ho-Baillie, Strontium-doped low-temperature-processed CsPbI2Br perovskite solar cells, ACS Energy Lett 2 (2017) 2319–2325.
[44] A. Mollar-Cuni, D. Ventura-Espinosa, S. Martín, Á. Mayoral, P. Borja, J.A. Mata, Stabilization of nanoparticles produced by hydrogenation of palladium-N-heterocyclic carbene complexes on the surface of graphene and implications in catalysis, ACS Omega 3 (2018) 15217–15228.
[45] H. Sezen, S. Suzer, Communication: Enhancement of dopant dependent x-ray photoelectron spectroscopy peak shifts of Si by surface photovoltage, J. Chem. Phys. 135 (2011) 162110.
[46] C. Rocks, V. Svrcek, T. Velusamy, M. Macias-Montero, P. Maguire, D. Mariotti, Type-I alignment in MAPbI3 based solar devices with doped-silicon nanocrystals, Nano Energy 50 (2018) 245–255.
[47] G. Rajendra Kumar, A. Dennyson Savariraj, S.N. Karthick, S. Selvam, B. Balamuralitharan, H.J. Kim, K.K. Viswanathan, M. Vijaykumar, K. Prabakar, Phase transition kinetics and surface binding states of methylammonium lead iodide perovskite, Phys. Chem. Chem. Phys. 18 (2016) 7284–7292.
[48] Z. Ahmad, M.A. Najeeb, R.A. Shakoor, A. Alashraf, S.A. Al-, S.A. Al-Muhtaseb, A. Soliman, M.K. Nazeeruddin, Instability in CH 3 NH 3 PbI 3 perovskite solar cells due to elemental migration and chemical composition changes, Sci. Rep. 7 (2017) 1–8.